# Absolute molecular density determinations by direct referencing of a quantum cascade laser to an optical frequency comb

**A. Castrillo · A. Gambetta · D. Gatti · G. Galzerano · P. Laporta · M. Marangoni · L. Gianfrani**

**Abstract** We propose a new approach to chemical gas analysis in the gas phase by direct referencing of a quantum cascade laser (QCL) to a near-infrared optical frequency comb. The concept was demonstrated through measurements of $CO_2$ molecular densities, reaching a precision of 0.2 %. Thanks to the robust phase lock of the QCL to the comb, absorption profiles could be recorded with high accuracy and repeatability by tuning the repetition rate of the comb. Such a scheme gave us the opportunity to test a variety of semiclassical line-shape models, accounting for both Dicke narrowing and speed-dependent effects. The success of the speed-dependent Nelkin–Ghatak model, with a hypergeometric dependence of the pressure broadening coefficient on the absorber speed, was demonstrated. Finally, the dependence of molecular density determinations on the choice of the line-shape model was investigated, thus demonstrating the inadequacy of the Voigt profile.

## 1 Introduction

We are at the beginning of a new age for chemical gas analysis in the gas phase, thanks to the recent progress of optical frequency comb spectroscopy. Laser absorption spectroscopy is a well-established technique for chemical gas analysis. For many years, after the invention of room-temperature semiconductor diode lasers, we have seen a variety of methodological and technical developments aimed at increasing the detection sensitivity to extreme levels, especially when combined with high-finesse optical cavities. The main limitation, however, of these laser-based analyzers is the inability to measure broadband spectra. Based upon mode-locked femtosecond lasers, an optical frequency comb synthesizer (OFCS) provides hundreds of thousands of sharp, equally spaced, spectral components, distributed across hundreds of nanometers. In the last few years, OFCSs are finding an increasing number of new applications in different research fields [1]. The main motivation for their invention was to provide a direct and phase-coherent link between optical and microwave domains, thus allowing for precision measurements of optical frequencies. As a result, the field of frequency metrology has received a tremendous impulse in the past two decades [2]. Beyond the main application, combs are being explored as broadband calibration sources for astronomical spectrographs [3] or for multiple-wavelength interferometry providing absolute distance measurements [4]. Used in the reverse direction, so as to divide the optical domain down to the RF regime, the comb technology also shows a huge potential for low-phase-noise microwave generation [5]. Coming back to chemical analysis, the unique properties of a frequency comb have been recently exploited to propose a radically new class of absorption spectrometers, capable of combining broadband operation with high spectral resolution, and short acquisition times with high detection sensitivities, encompassing absolute wavelength calibration [6]. Cavity-enhanced direct frequency comb spectroscopy with shot-noise-limited absorption sensitivity is nowadays possible and it is ready for be-

A. Castrillo (✉) · L. Gianfrani
Dipartimento di Scienze Ambientali, Seconda Università di Napoli, via Vivaldi 43, 81100 Caserta, Italy
e-mail: antonio.castrillo@unina2.it

A. Gambetta · D. Gatti · M. Marangoni
Dipartimento di Fisica, Politecnico di Milano, Campus Point – Polo di Lecco, via Ghislanzoni 24, 23900 Lecco, Italy

G. Galzerano · P. Laporta
IFN-CNR, Dipartimento di Fisica, Politecnico di Milano, Piazza L. da Vinci 32, 20133 Milano, Italy
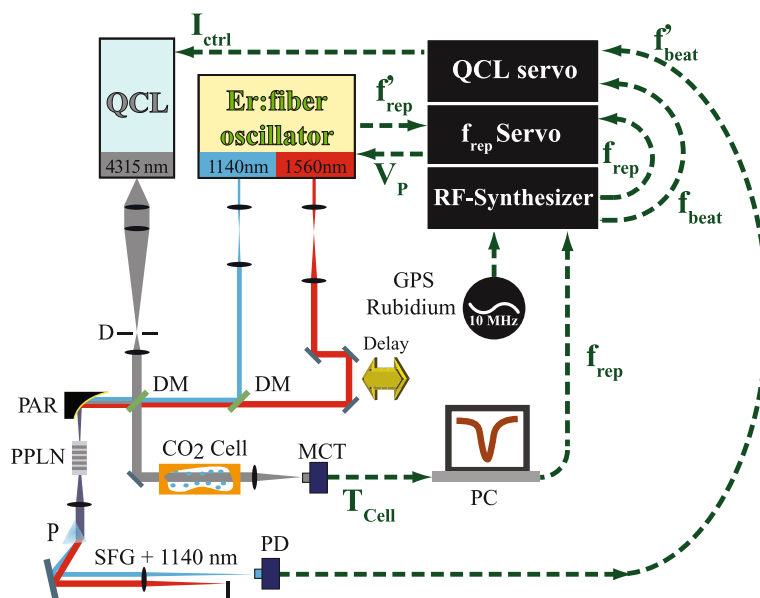
**Fig. 1** Experimental setup for comb-referenced scanning of the QCL frequency and absorption profiles' acquisition. D: diaphragm, DM: dichroic mirror, PAR: 90° off-axis parabolic mirror, PPLN: periodically poled lithium niobate crystal, P: prism, PC: personal computer, PD: amplified InGaAs photodetector, MCT: Peltier-cooled mercury–cadmium–telluride detector (active region of about 250-μm diameter and nearly 2-MHz bandwidth), $T_{cell}$: cell transmittance; $V_P$: voltage control signal for piezoactuation of the oscillator cavity length; $I_{ctrl}$: current correction signal for the active control of the QCL frequency; $f_{rep}$: variable laser repetition rate (set by the computer), $f_{beat}$: offset frequency used for stabilization of the beat note, $f'_{rep}$ and $f'_{beat}$ are the actual beating and repetition rates

ing employed in molecular fingerprinting and trace-gas detection [7]. In a different approach, a tunable laser, such as a semiconductor diode laser in the near infrared, can be used to probe the molecular species of interest while the OFCS serves simply as a frequency ruler against which the tunable laser is calibrated [8, 9]. For those applications in which the highest metrological qualities are required, in order to address the issue of traceability, but also to meet the data quality objectives as defined by the Global Atmosphere Watch programme of the World Meteorological Organization,[1] this second approach (known as comb-calibrated laser spectroscopy) shows the highest potential [10–12].

In a recent paper, we have performed direct referencing of a distributed feedback (DFB) quantum cascade laser (QCL) to a near-infrared frequency comb and demonstrated how traceable and accurate spectroscopic data could be retrieved in the mid-infrared spectral region [13]. Since the QCL was phase locked to the comb, by tuning the comb repetition rate it was possible to scan the QCL frequency across a given absorption line, thus producing an absorption spectrum with a highly accurate, absolute, and repeatable frequency axis. In the present paper, we propose the same technology as a traceable laser-based method for measurement of $CO_2$ amount of substance, allowing for direct and absolute measurements of molecular densities without

the need of routine calibration with certified gas mixtures. The absolute nature of the method derives from the use of a direct absorption detection scheme, on the one hand, and from the absolute frequency scale guaranteed by the OFCS, on the other hand. Exploiting the excellent linearity of the frequency scale underlying the molecular absorption profile, we were also able to evidence speed-dependent effects, which had to be taken into account in order to successfully describe the observed $CO_2$ line-shape. Finally, we analyzed the influence of the choice of the line-shape model on molecular densities' retrieval.

## 2 Experimental setup

The experimental apparatus used for the present study is identical to that briefly described in Ref. [14]. Here we provide a much more detailed description of the apparatus, also highlighting certain aspects of the methodology as they apply to the measurement of the molecular density. A diagram of the setup is shown in Fig. 1.

Our frequency comb, extensively described in Ref. [15], is based upon a 100-MHz femtosecond Er:fiber oscillator (Toptica model FFS [16]), with two phase-coherent amplified outputs: the one, centered at 1.55-μm wavelength, delivers nearly 250 mW of average power, while the other provides nearly 160 mW of supercontinuum (SC) light, whose spectral extension can be tuned by modification of the chirp

of the pulses injected in the SC fiber [17]. The OFCS is equipped with piezoelectric stages and locking electronics so as to enable the stabilization of the repetition rate, which could be continuously tuned between 99.9 and 100.1 MHz. The QCL was a cw liquid-nitrogen-cooled DFB laser from Alpes Laser [17], emitting on a single longitudinal mode and providing an optical power of up to 20 mW, with a threshold current of ∼90 mA. It was driven by a commercial power supply (model LDC-3744B, from ILX Lightwave [17]) with current noise limited to 10 µA root-mean square (rms). The output beam was collimated by employing a 2-in.-diameter biconvex $MgF_2$ lens, with a focal length of 50 mm. A telescope composed by a pair of lenses with 200- and 50-mm focal lengths was used to reduce by a factor of four the beam size. To minimize the effect of the aberrations introduced by the collimating lens, a 100-µm-wide pinhole provided spatial filtering in the focal plane of the telescope. The QCL beam and the two outputs of the Er:fiber oscillator are combined by means of a $CaF_2$-based dichroic mirror. The three beams were then focused with a 90° off-axis parabolic mirror (focal length of 50 mm) into a 4-mm-long PPLN crystal, operating at a fixed temperature of about 298 K. In the crystal a sum-frequency-generation (SFG) process occurred between the 4.3- and the 1.55-µm radiations, thus providing the up-conversion of the QCL beam to the 1.14-µm-wavelength region. After spectral filtering of the broader SC and focusing with a 300-mm lens, the beat note between the two signals (the SC centered at 1.14 µm and the sum-frequency radiation) was observed by means of a 125-MHz-bandwidth InGaAs detector (New Focus model 1811-FS [17]).

Direct referencing of the QCL to the OFCS was implemented by phase locking the beat note to a 15-MHz reference signal generated from a synthesizer, which in turn was synchronized by a GPS-disciplined rubidium microwave standard (model 4410A, from Symmetricom [17]). The phase lock was achieved by combination of a 200-kHz-bandwidth phase detector (model PDF-200w, from RFbay [17]) with a FPGA-based proportional–integrative–derivative (PID) servo loop, acting on the QCL injection current. A control bandwidth of 2 kHz, as limited by the input bandwidth of the QCL current driver, was achieved. The dynamic range of the servo loop allowed for a robust locking. Thus, by changing the repetition rate by 30 kHz a continuous variation of the QCL frequency of about 20 GHz was obtained.

By indicating with $f_{rep}$ the repetition rate, the corresponding mid-IR frequency, $f_{QCL}$, could be retrieved using the following equation:

$$f_{QCL} = \pm f_{beat} + K f_{rep}, \tag{1}$$

where $K$ is an integer number and $f_{beat}$ equals the 15-MHz frequency offset. The correct sign for $f_{beat}$ was assessed by monitoring the sign of the shift of the beat note upon changing the repetition rate when the QCL was working in a free-running regime. Furthermore, the mode number $K$ was unambiguously established by comparing the emission frequency of the QCL with the center frequency value reported for the investigated transition in the HITRAN database [18]. Indeed, for the absorption line subject of the present study, the accuracy given by HITRAN is lower than 30 MHz, i.e. lower than half the repetition rate. At this point, it is worth noting that the advantage of this approach is that the carrier-envelope-offset frequency $f_{ceo}$ does not come into play and does not need to be controlled. In fact, as previously shown by Amy-Klein et al. [19], since the frequency of the SFG radiation is ruled by the equation $f_{SFG} = f_{ceo} + N \times f_{rep} + f_{QCL}$, while the frequency of the SC modes are given by $f_{SC} = f_{ceo} + M \times f_{rep}$ ($N$ and $M$ being two integer numbers, with $M > N$), their difference gives Eq. (1), with $K = M - N$, where $f_{ceo}$ cancels out.

Finally, the interrogation of the gaseous sample was performed by sending a small part of the QCL power (lower than 100 µW, so as to neglect any nonlinear interaction between the laser and the gaseous sample) inside a 12-cm-long stainless-steel cell, filled with pure $CO_2$. A turbomolecular pump was used to evacuate the cell. The gas pressure was measured by means of a capacitive gauge with a relative accuracy of $2.5 \times 10^{-3}$. A calibrated platinum resistance thermometer (Pt-100), connected to a $6\frac{1}{2}$-digit multimeter, was stuck on the gas cell wall to measure the gas temperature with an accuracy of a few tens of mK.

The intensity of the beam passing through the cell was monitored by a Peltier-cooled MCT photovoltaic detector. All the instruments were interfaced to the computer and a properly developed LabVIEW© code was used to perform a step-by-step frequency scan and acquire, for each step, the transmitted signal.

## 3 Spectral analysis

The laser power attenuation in the presence of an absorbing medium is ruled by the well-known Lambert–Beer law

$$P(\tilde{\nu}) = P_0(\tilde{\nu}) \exp\left[-S(T)g(\tilde{\nu} - \tilde{\nu}_0)nL\right], \tag{2}$$

where $P_0(\tilde{\nu})$ is the incident power, $S(T)$ is the transition strength (in cm/molecule) at the gas temperature $T$, $\tilde{\nu}$ is the laser wavenumber (in $cm^{-1}$), $\tilde{\nu}_0$ is the line-center wavenumber, $L$ is the absorption path length (in cm), $n$ is the molecular gas density (in molecules/$cm^3$), and $g(\tilde{\nu} - \tilde{\nu}_0)$ is the normalized line-shape function (in cm).

Introducing the spectral absorbance $A(\tilde{\nu}) = -\ln[P(\tilde{\nu})/P_0(\tilde{\nu})]$, Eq. (2) takes the following integral form:

$$\int_{-\infty}^{\infty} A(\tilde{\nu})\,d\tilde{\nu} = S(T)nL \equiv A_{line}, \tag{3}$$

where the quantity $A_{line}$, known as integrated absorbance, represents the observable of interest in any recorded spectrum. In principle, an absolute determination of $n$ can be carried out using Eq. (3), provided that the path length and the transition strength are known. For this purpose, a refined interpolation of the spectrum is an indispensable prerequisite.

Spectral analysis was performed by using a variety of semiclassical models, whose physical basis and mathematical form are described in [20, 21]. In this section, we limit the report to the basic equations that were implemented in the line-fitting procedure. The first models we considered in the spectral analysis were the Voigt profile (VP), the Galatry profile (GP), and the Nelkin–Ghatak profile (NGP), mathematically expressed by:

$$g_{VP}(x, y) = \frac{1}{\sqrt{\pi}} \Re \{ w(x, y) \}, \tag{4}$$

$$g_{GP}(x, y, z) = \frac{1}{\sqrt{\pi}} \Re \left\{ \int_0^\infty \exp\left[ -(ix + y)\tau \right. \right.$$
$$\left. \left. + \frac{1}{2z^2}\left( 1 - z\tau - e^{-z\tau} \right) \right] d\tau \right\}, \tag{5}$$

$$g_{NGP}(x, y, \zeta) = \frac{1}{\sqrt{\pi}} \Re \left\{ \frac{[w(x, y + \zeta)]}{1 - \sqrt{\pi}\zeta[w(x, y + \zeta)]} \right\}. \tag{6}$$

Here $\Re$ stands for the real part of the quantity that follows and $w(a, b)$ is the complex probability function. Following the approach proposed in Ref. [22], $\tau$ represents the dimensionless time and $x, y, z, \zeta$ are non-dimensional variables related to the 1/e Doppler half-width $\Delta\nu_D = \frac{\tilde{\nu}_0}{c}\sqrt{2k_B T/m_A}$ ($k_B$ is the Boltzmann constant and $m_A$ is the absorber mass), the effective frequency of phase-changing collisions $\Gamma$, the effective frequency of velocity-changing collisions $\beta$, and the total collision frequency $\Omega$, through the following equations:

$$x = \frac{(\tilde{\nu} - \tilde{\nu}_0)}{\Delta\nu_D}, \qquad y = \frac{\Gamma}{\Delta\nu_D},$$
$$z = \frac{\beta}{\Delta\nu_D}, \qquad \zeta = \frac{\Omega}{\Delta\nu_D}.$$

The Voigt function is a convolution of Gaussian and Lorentzian profiles, providing a 'first-order' representation of both Doppler and collisional broadening, considered as statistically independent. The GP and NGP models allow one to take into account the Dicke narrowing effect, under the soft- and hard-collision approximations, respectively. This effect constitutes a correction to the Doppler broadening caused by the averaging effect of velocity-changing collisions. In many cases, the Dicke effect alone is not sufficient to justify the observed narrowing of the Doppler width. Speed dependence of collisional parameters has to be considered, leading to the so-called speed-dependent Voigt profile (SDVP), speed-dependent Galatry profile (SDGP), and speed-dependent Nelkin–Ghatak profile (SDNGP). It is worth noting that speed dependence of collisional width and shift may introduce line narrowing and asymmetry near the line center.

In the formalism developed by Berman [23] and Pickett [24], it is assumed that the collisional broadening and shifting have power-law dependences on the relative speed of the absorber/perturber system, with an exponent determined by the interaction potential, which in turn can be written in the form $V(r) = C_q/r_q$, where $C_q$ is a constant. Hence, the speed dependence of the collisional broadening parameter can be described by the confluent hypergeometric function, leading to the following profiles:

$$g_{SDVP}(x, y, B)$$
$$= \frac{2}{\pi\sqrt{\pi}} \times \Re \left\{ \int_{-\infty}^{+\infty} du\, u e^{-u^2} \left\{ \arctan\left[ \frac{x+u}{yB(\alpha, u)} \right] \right.\right.$$
$$\left.\left. + \frac{i}{2} \ln\left[ 1 + \left( \frac{x+u}{yB(\alpha, u)} \right)^2 \right] \right\} \right\}, \tag{7}$$

$$g_{SDGP}(x, y, z, B)$$
$$= \frac{4}{\pi\sqrt{\pi}} \times \Re \left\{ \int_0^{+\infty} d\tau \exp\left[ -\left( \frac{1}{2z} \right)^2 (2z\tau - 3 \right.\right.$$
$$\left. + 4e^{-z\tau} - e^{-2z\tau}) \right]$$
$$\times \int_0^\infty du\, u^2 e^{-u^2} \text{sinc}\left[ \frac{u(1 - e^{-z\tau})}{z} \right]$$
$$\left. \times \exp\left[ -ix\tau - yB(\alpha, u)\tau \right] \right\}, \tag{8}$$

$$g_{SDNGP}(x, y, \zeta, B) = \Re \left\{ \left[ \frac{\Phi(x, y, \zeta)}{1 - \pi\zeta\Phi(x, y, \zeta)} \right] \right\}, \tag{9}$$

where

$$u = \frac{v}{\bar{v}}, \qquad \alpha = \frac{m_A}{m_P}, \qquad \text{sinc}(a) = \frac{\sin(a)}{a},$$

$$B(\alpha, u) = (1 + \alpha)^{-(q-3)/(2q-2)} \times M\left( -\frac{q-3}{2q-2}, \frac{3}{2}, -\alpha u^2 \right),$$

$$\Phi(x, y, \zeta) = \frac{2}{\pi\sqrt{\pi}} \int_{-\infty}^\infty du\, u e^{-u^2} \left\{ \arctan\left( \frac{x+u}{yB(\alpha, u) + \zeta} \right) \right.$$
$$\left. + \frac{i}{2} \ln\left[ 1 + \left( \frac{x+u}{yB(\alpha, u) + \zeta} \right)^2 \right] \right\}.$$

In these equations, $M(a, b, c)$ is the confluent hypergeometric function, $v$ and $\bar{v} = \sqrt{2k_B T/m_A}$ are the speed and the most probable speed of the absorber, and $m_P$ is the perturber mass.

It is relevant to note that we omitted the speed dependence of the pressure shift, as we did not find any significant asymmetry in the measured spectra. This is evidenced by the fit residuals, as will be discussed in Sect. 4. Moreover, we assumed a quadrupole–quadrupole interaction between self-colliding $CO_2$ molecules, thus using $q = 5$.

## 4 Results and discussion

In order to test the performance of the phase-locking loop, as well as the overall stability of the spectrometer, we recorded the absorption spectra resulting from 20 consecutive scans of the laser frequency across the P15f absorption line at a pressure of about 8.2 Torr and a temperature of 298 K. The overlapped spectra are shown in Fig. 2. Each laser scan was ~2.8-GHz wide as obtained with 4000 steps of 1 Hz each, for an acquisition time of about 5 min. Spectral analysis was performed through a nonlinear least-squares fit based on Eq. (2), with the SDNGP profile, and using a Levenberg–Marquardt algorithm under the MATLAB$^{\copyright}$ environment.
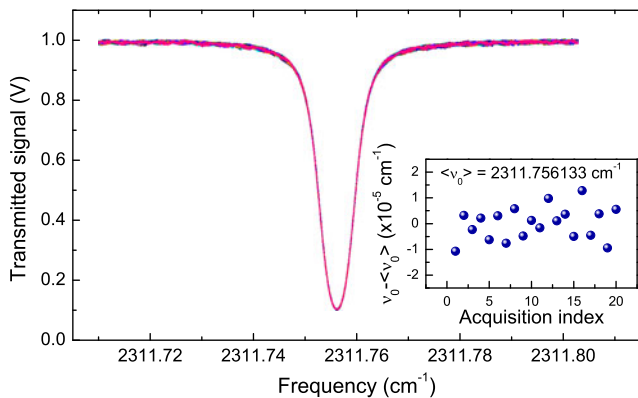


**Fig. 2** Absorption spectra resulting from 20 repeated acquisitions at a $CO_2$ pressure of about 8.2 Torr, in coincidence with the P15f line of the $(0, 2^2, 0) \rightarrow (0, 2^2, 1)$ band. The *inset* quantifies the dispersion of the retrieved line-center frequencies. A 1-$\sigma$ fluctuation of 190 kHz was found. As for the vertical scale, the stability is about 1 %, without signal averaging, mainly limited by periodic fluctuations of the baseline due to spurious etalon effects
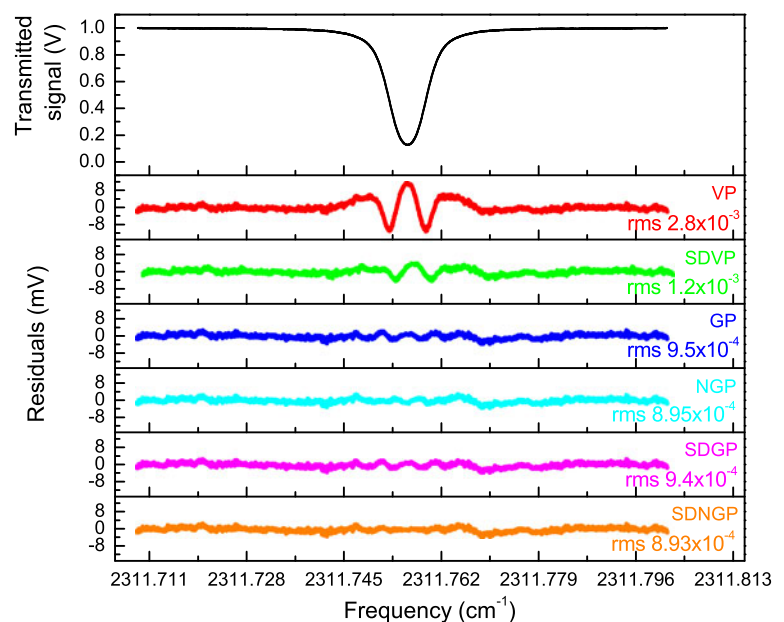
So doing, we could quantify the frequency stability of our spectrometer, over a time span of about 30 min. A 1-$\sigma$ fluctuation of 190 kHz was found for the line-center frequency, corresponding to a relative stability of $2.7 \times 10^{-9}$. This is only slightly larger with respect to that expected on the basis of the stability of the comb repetition rate, and partially limited by the signal-to-noise ratio (SNR) of the recorded spectra. Spurious etalon effects surely increase the statistical uncertainty in the retrieved line-center frequency, as provided by the fitting procedure. However, in the short term, no frequency drift was evidenced, further demonstrating the rather good frequency stability of our comb-calibrated spectrometer.

Figure 3 shows the transmission spectrum resulting from averaging over 10 consecutive acquisitions. Such a spectrum was interpolated by using all the models of Eqs. (4)–(9), considering $y$, $z$, and $\zeta$, as well as $A_{line}$ and $\tilde{v}_0$, as floating parameters. We kept fixed the Doppler width $\Delta v_D$ to the expected value on the basis of the measured temperature. As for the incident power, we modeled its dependence on the laser frequency with a second-order polynomial to take into account the laser power modulation during the QCL scans. Subsequently, the retrieved background was removed from the experimental spectra. Figure 3 also shows fit residuals for VP, SDVP, GP, NGP, SDGP, and SDNGP. As evidenced by the clear 'w' structure in the residuals, VP fails to reproduce the measured spectrum, owing to the occurrence of line-narrowing mechanisms. Indeed, adding the speed dependence to the Voigt model, namely using SDVP, the rms value of the residuals reduces by nearly a factor of two, although the 'w'-shaped structure still remains clearly visible. Line profiles that take into account the Dicke-narrowing effect (GP and NGP) lead to vastly re-

**Fig. 3** Example of an experimental profile, corresponding to the P15f absorption line at a pressure of 8.2 Torr. The residuals are also shown, as a result of a nonlinear least-squares fit to VP, NGP, and GP and to their speed-dependent versions (SDVP, SDGP, and SDNGP)

duced residuals. However, the Dicke effect alone appears to be unable to completely explain the observed line narrowing, as small and rather regular structures still persist in the residuals, around the center of the line. Of these, the one relative to GP presents a rms value higher than NGP, thus confirming that the hard-collision model is the most appropriate choice when the absorber and perturber have equal masses. This hypothesis is further confirmed by the results obtained with the last two profiles, namely SDGP and SDNGP. Indeed, the addition of the narrowing effect caused by the speed dependence of the collisional width to the GP model does not translate into a complete removal of the structures, SDGP having a rms value comparable to that of GP. On the contrary, the SDNGP and NGP models are the only models capable of fitting the spectrum within the experimental noise, the rms value of their residuals being below $9 \times 10^{-4}$. It must be said, however, that the SDNGP profile appears to be superior as it completely removes the residual deviations appearing around the line center that can be seen with NGP. This conclusion is in full agreement with the results recently published by Long et al. [25], showing that also in the case of air-broadened, near-infrared $CO_2$ spectra, the profile that better reproduces the absorption spectra is SDNGP.

Another physical argument supporting the hypothesis that the soft-collision model is unsatisfactory in reproducing the $CO_2$ experimental spectra is related to the collisional narrowing parameters that were retrieved from the fits. In both soft- and hard-collision models, previous experiments have shown that an upper limitation to the effective frequency of velocity-changing collisions is given by the diffusion parameter defined as $k_B T / 2\pi m_A D$, where $D$ is the mass diffusion coefficient [26]. From the analysis of our spectra, we found that the $\beta$ value retrieved with GP is higher than expected from the diffusion theory, in agreement with the results obtained in the near-infrared spectrum of $CO_2$ by Casa et al. [27]. On the other hand, the total collision frequency $\Omega$ determined by using the NGP is about four times smaller than the diffusion parameter. For completeness, in Table 1, we report the values of the $\Gamma$, $\beta$, and $\Omega$ frequencies obtained from the fits.

As a result of the line-fitting procedure, the $CO_2$ molecular density $n$ can also be determined, provided that the transition strength of the selected line and the absorption path length are known. The former can be derived according to the following equation [28]:

$$S(T) = S(T_0) \frac{Q(T_0)}{Q(T)} \frac{[1 - \exp(-\frac{hc\tilde{v}_0}{k_B T})]}{[1 - \exp(-\frac{hc\tilde{v}_0}{kT_0})]}$$
$$\times \exp\left[-hc\frac{E''}{k_B}\left(\frac{1}{T} - \frac{1}{T_0}\right)\right], \quad (10)$$

where $S(T_0)$ is the line strength at the reference temperature $T_0 = 296$ K, taken from the HITRAN database [18], $h$ is the

**Table 1** Comparison of spectroscopic parameters derived from various line profiles obtained at a pressure $P = 8.2$ Torr and a temperature $T = 298$ K. Statistical uncertainties, reported in parentheses, correspond to one standard error

| | $\Gamma$ (cm$^{-1}$) | $\beta$ (cm$^{-1}$) | $\Omega$ (cm$^{-1}$) |
|---|---|---|---|
| VP | 0.00116(4) | | |
| GP | 0.001162(2) | 0.00332(5) | |
| NGP | 0.001143(2) | | $4.05(5) \times 10^{-4}$ |
| SDVP | 0.001183(2) | | |
| SDGP | 0.001165(2) | $2.35(7) \times 10^{-4}$ | |
| SDNGP | 0.001153(2) | | $1.52(4) \times 10^{-4}$ |

Planck constant, $c$ is the vacuum speed of light, $E''$ is the lower-state energy of the transition, and the quantity $Q(T)$ is the total internal partition function of the $CO_2$ molecule at the temperature $T$. The measurement of the path length was accurately performed by means of an interferometric method, following the procedure described in Ref. [29]. Very briefly, we mounted a Michelson interferometer in such a way that the cell was placed within one of the interferometer arms. The cell was filled with standard air at increasing pressures, while keeping the temperature constant. This procedure modifies the optical-path difference between the two arms and produces in the recombination arm of the interferometer a sequence of fringes that can be easily acquired and interpolated to retrieve the overall amount of phase shift. Such a shift is proportional to the geometrical length of the cell and to the refractive-index variation. By exploiting the known dependence of the refractive index on air pressure and temperature [30], a length value of $11.93 \pm 0.03$ cm was obtained, the uncertainty being mainly limited by the accuracy of the pressure gauge.

The performance of our comb-calibrated spectrometer, in terms of precision in molecular density determinations, was investigated through a variety of experimental tests on different time scales. We carried out 13 series of 20 repeated acquisitions, over three subsequent days, under identical experimental conditions. For each spectrum, the $n$ value was retrieved according to the fitting procedure described above, using the SDNGP model. The outcomes of one dataset are shown in Fig. 4. Here the mean value was found to be $2.568 \times 10^{17}$ molecules/cm$^3$, with a 1-$\sigma$ statistical uncertainty of 0.2 %. In the other series of measurements, nearly equal standard deviations were observed. Hence, this value quantifies the precision level over a total acquisition time of about 30 min. On the other hand, the mean values changed between $2.544 \times 10^{17}$ molecules/cm$^3$ and $2.603 \times 10^{17}$ molecules/cm$^3$, thus indicating a lower precision in the medium term. This is shown in Fig. 5, in which the mean values resulting from all datasets exhibit a reproducibility of about 0.5 %. We draw the reader's attention to the fact that the mean value of $n$, as shown in
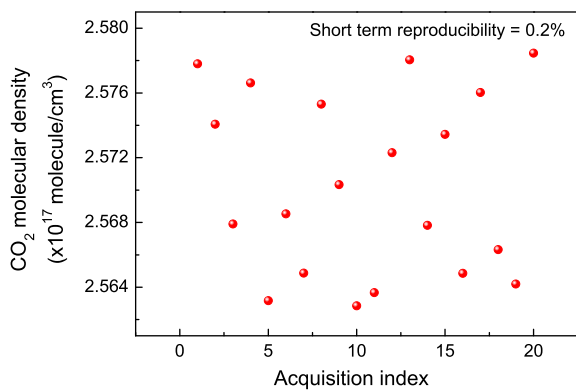
**Fig. 4** Results of 20 repeated determinations of the $CO_2$ molecular density, performed scanning the laser frequency across the P15f line. The gas pressure was 8.2 Torr and the line-shape profile used in the analysis was the SDNGP
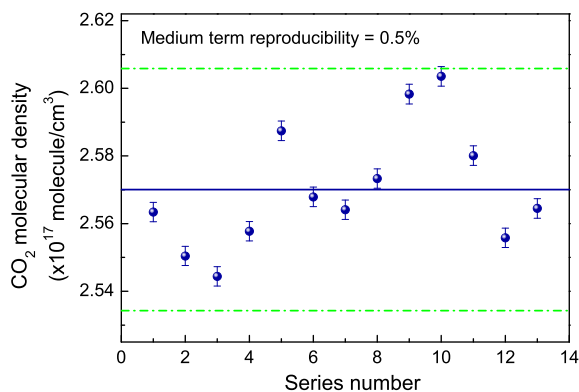


**Fig. 6** $CO_2$ molecular density determinations, calculated as mean values over 20 consecutive laser scans, obtained from all the line profiles considered in this work. *Each error bar* represents one standard error. The *solid line* is the mean calculated over all the retrieved $n$ values obtained using the SDNGP. The *dash-dot lines* represent the 3-$\sigma$ confidence interval



**Fig. 5** Results of a medium-term reproducibility test of our comb-calibrated spectrometer. Prior to each dataset, the cell was evacuated and filled with a $CO_2$ sample at a pressure of 8.2 Torr. *Each point* represents the mean value of 20 repeated determinations, the error bar being one standard error. The *solid line* and the *two dash-dot lines* show the mean value over the 13 series and the 2-$\sigma$ variation interval, respectively

meanings of the other investigated profiles, the determination of the molecular gas density appears to be quite independent of the choice of the line-shape model, at least at the present precision level. It is noteworthy that this outcome is in full agreement with our previous study performed on several near-infrared absorption lines of the $\nu_1 + 2\nu_2 + \nu_3$ band [27]. It also agrees with recent findings from Lisak et al. on the visible spectrum of molecular oxygen [31].

## 5 Conclusions

We developed a comb-calibrated QCL spectrometer enabling traceable determinations of molecular number densities in gaseous samples. The reproducibilities were found to be 0.2 and 0.5 %, over time spans of about 30 min and 3 days, respectively. The concept was demonstrated on $CO_2$ at 4.3 μm, but could be easily extended to many other molecules in the so-called fingerprint region, since widely tunable QCLs are commercially available in the whole 3–12-μm spectral range. The absorption profile in coincidence with the P15f line of the $CO_2$ $(0, 2^2, 0) \rightarrow (0, 2^2, 1)$ hot band was observed with a high spectral fidelity, given by the absolute nature of the frequency axis. As a result of a careful spectral analysis, we found that the speed-dependent Nelkin–Ghatak model was the only one capable of reproducing the experimental profiles within the noise level. We also considered the influence of the choice of the line-shape model in retrieving molecular number densities, showing the failure of the Voigt convolution, at the present operation conditions of gas temperature and pressure. On the other hand, the other profiles yield consistent values for the integrated absorbance and, consequently, for the molecular density.

Similarly, the extension to the detection of rare isotopologues would be possible when using highly sensitive detection schemes, such as cavity ring-down spectroscopy. In this

Fig. 5, namely $2.570 \times 10^{17}$ molecules/cm$^3$, is about 3 % lower than that expected on the basis of the thermodynamic operation conditions. This is not surprising, however, and cannot quantify the accuracy of the proposed methodology. In fact, the transition strength used for our determinations, taken from the HITRAN database [18], was $4.649 \times 10^{-21}$ cm/molecule with an uncertainty between 5 and 10 %, which is well above the observed discrepancy.

Finally, we investigated the possible impact of the choice of the line-shape model on the molecular density determination. The spectra of Fig. 2 were analyzed by using all the profiles previously described. In Fig. 6, the resulting $n$ values and the associated uncertainties are shown. As can be seen, all the line-shape models, except for VP, yield $n$ values that are consistent within three standard errors. In particular, VP systematically underestimates the molecular density by more than 1 %. Thus, excluding the Voigt convolution, despite the strong differences between the physical
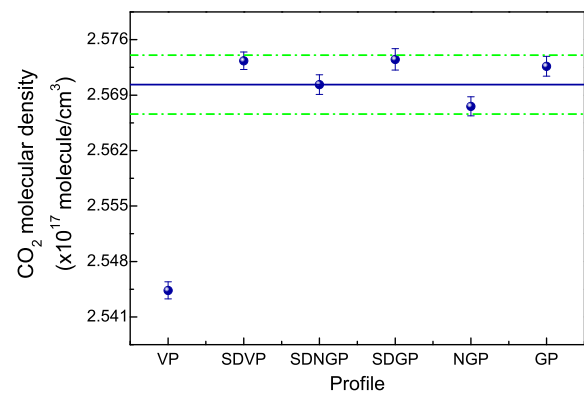
respect, we could benefit from the successful experiments recently performed by other groups [32, 33].

Selecting a much stronger $CO_2$ line, our study could be repeated in the presence of gravimetrically prepared gas mixtures, with the aim of testing the achievable accuracy level, following the approach recently reported for the spectroscopic determination of the CO amount of substance fraction [34].

## References

1. N.R. Newbury, Nat. Photonics **5**, 186 (2011)
2. S.A. Diddams, J. Opt. Soc. Am. B **27**, 51 (2010)
3. T. Steinmetz, T. Wilken, C. Araujo-Hauck, R. Holzwarth, T.W. Hänsch, L. Pasquini, A. Manescau, S. D'Odorico, M.T. Murphy, T. Kentischer, W. Schmidt, Th. Udem, Science **321**, 1335 (2008)
4. I. Coddington, W.C. Swann, L. Nenadovic, N.R. Newbury, Nat. Photonics **3**, 351 (2009)
5. F. Quinlan, T.M. Fortier, M.S. Kirchner, J.A. Taylor, M.J. Thorpe, N. Lemke, A.D. Ludlow, Y. Jiang, S.A. Diddams, Opt. Lett. **36**, 3260 (2011)
6. S.A. Diddams, L. Hollberg, V. Mbele, Nature **445**, 627 (2007)
7. A. Foltynowicz, T. Ban, P. Maslowski, F. Adler, J. Ye, Phys. Rev. Lett. **107**, 233002 (2011)
8. Th. Udem, J. Reichert, R. Holzwarth, T.W. Hänsch, Phys. Rev. Lett. **82**, 3568 (1999)
9. P. Balling, M. Fischer, P. Kubina, R. Holzwarth, Opt. Express **13**, 9196 (2005)
10. K.M.T. Yamada, A. Onae, F.-L. Hong, H. Inaba, H. Matsumoto, Y. Nakajima, F. Ito, T. Shimizu, J. Mol. Spectrosc. **249**, 95 (2008)
11. S. Bartalini, P. Cancio, G. Giusfredi, D. Mazzotti, P. De Natale, S. Borri, I. Galli, T. Leveque, L. Gianfrani, Opt. Lett. **32**, 988 (2007)
12. P. Malara, P. Maddaloni, G. Gagliardi, P. De Natale, Opt. Express **16**, 8242 (2008)
13. A. Gambetta, D. Gatti, A. Castrillo, G. Galzerano, P. Laporta, L. Gianfrani, M. Marangoni, Appl. Phys. Lett. **99**, 251107 (2011)
14. D. Gatti, A. Gambetta, A. Castrillo, G. Galzerano, P. Laporta, L. Gianfrani, M. Marangoni, Opt. Express **19**, 17520 (2011)
15. A. Gambetta, D. Gatti, A. Castrillo, N. Coluccelli, G. Galzerano, P. Laporta, L. Gianfrani, M. Marangoni, Appl. Phys. B doi:10.1007/s00340-012-4947-3
16. F. Tauser, F. Adler, A. Leitenstorfer, Opt. Lett. **29**, 516 (2004)
17. The citation of a company's name is for information only and does not constitute an endorsement
18. L.S. Rothman, I.E. Gordon, A. Barbe, D.C. Benner, P.F. Bernath, M. Birk, V. Boudon, L.R. Brown, A. Campargue, J.-P. Champion, K. Chance, L.H. Coudert, V. Dana, V.M. Devi, S. Fally, J.-M. Flaud, R.R. Gamache, A. Goldman, D. Jacquemart, I. Kleiner, N. Lacome, W.J. Lafferty, J.-Y. Mandin, S.T. Massie, S.N. Mikhailenko, C.E. Miller, N. Moazzen-Ahmadi, O.V. Naumenko, A.V. Nikitin, J. Orphal, V.I. Perevalov, A. Perrin, A. Predoi-Cross, C.P. Rinsland, M. Rotger, M. Ŝimecková, M.A.H. Smith, K. Sung, S.A. Tashkun, J. Tennyson, R.A. Toth, A.C. Vandaele, J. Vander Auwera, J. Quant. Spectrosc. Radiat. Transf. **110**, 533 (2009)
19. A. Amy-Klein, A. Goncharov, M. Guinet, C. Daussy, O. Lopez, A. Shelkovnikov, C. Chardonnet, Opt. Lett. **30**, 3320 (2005)
20. R. Ciurylo, Phys. Rev. A **58**, 1029 (1998)
21. J.-M. Hartmann, C. Boulet, D. Robert, *Collisional Effects on Molecular Spectra* (Elsevier, Amsterdam, 2008)
22. P.L. Varghese, R.K. Hanson, Appl. Opt. **23**, 2376 (1984)
23. P.R. Berman, J. Quant. Spectrosc. Radiat. Transf. **12**, 1331 (1972)
24. H. Pickett, J. Chem. Phys. **73**, 6090 (1980)
25. D.A. Long, K. Bielska, D. Lisak, D.K. Havey, M. Okumura, C.E. Miller, J.T. Hodges, J. Chem. Phys. **135**, 064308 (2011)
26. E.D. Winn, Phys. Rev. **80**, 1024 (1950)
27. G. Casa, R. Wehr, A. Castrillo, E. Fasci, L. Gianfrani, J. Chem. Phys. **130**, 184306 (2009)
28. R.R. Gamache, L.S. Rothman, J. Mol. Struct. **517**, 407 (2000)
29. A. Castrillo, G. Gagliardi, G. Casa, L. Gianfrani, Phys. Rev. A **67**, 062503 (2003)
30. G. Bönsch, E. Potulski, Metrologia **35**, 133 (1998)
31. D. Lisak, P. Maslowski, A. Cygan, K. Bielska, S. Wojtewicz, M. Piwinski, J.T. Hodges, R.S. Trawinski, R. Ciurylo, Phys. Rev. A **81**, 042504 (2010)
32. J. Domyslawska, S. Wojtewicz, D. Lisak, A. Cygan, F. Ozimek, K. Stec, Cz. Radzewicz, R.S. Trawinski, R. Ciurylo, J. Chem. Phys. **136**, 024201 (2012)
33. I. Galli, S. Bartalini, S. Borri, P. Cancio, D. Mazzotti, P. De Natale, G. Giusfredi, Phys. Rev. Lett. **107**, 270802 (2011)
34. J.A. Nwaboh, O. Werhahn, D. Schiel, Appl. Phys. B **103**, 947 (2011)